



**HAL**  
open science

# Nanocomposite thin film of Ag nanoparticles embedded in amorphous Al<sub>2</sub>O<sub>3</sub> on optical sensors windows: Synthesis, characterization and targeted application towards transparency and anti-biofouling

Claire Tendero, Ana-Maria Lazar, Diane Samélor, Olivier Debieu, Vassilios Constantoudis, George Papavieros, Aurélie Villeneuve, Constantin Vahlas

## ► To cite this version:

Claire Tendero, Ana-Maria Lazar, Diane Samélor, Olivier Debieu, Vassilios Constantoudis, et al.. Nanocomposite thin film of Ag nanoparticles embedded in amorphous Al<sub>2</sub>O<sub>3</sub> on optical sensors windows: Synthesis, characterization and targeted application towards transparency and anti-biofouling. *Surface and Coatings Technology*, 2017, 328, pp.371-377. 10.1016/j.surfcoat.2017.08.061 . hal-01623527

**HAL Id: hal-01623527**

**<https://hal.science/hal-01623527>**

Submitted on 26 Oct 2017

**HAL** is a multi-disciplinary open access archive for the deposit and dissemination of scientific research documents, whether they are published or not. The documents may come from teaching and research institutions in France or abroad, or from public or private research centers.

L'archive ouverte pluridisciplinaire **HAL**, est destinée au dépôt et à la diffusion de documents scientifiques de niveau recherche, publiés ou non, émanant des établissements d'enseignement et de recherche français ou étrangers, des laboratoires publics ou privés.



## Open Archive Toulouse Archive Ouverte (OATAO)

OATAO is an open access repository that collects the work of Toulouse researchers and makes it freely available over the web where possible.

This is an author-deposited version published in: <http://oatao.univ-toulouse.fr/>  
Eprints ID: 18564

**To link to this article:** DOI: [10.1016/j.surfcoat.2017.08.061](https://doi.org/10.1016/j.surfcoat.2017.08.061)  
URL: <http://dx.doi.org/10.1016/j.surfcoat.2017.08.061>

**To cite this version:** Tendero, Claire and Lazar, Ana-Maria and Samélor, Diane and Debieu, Olivier and Constantoudis, Vassilios and Papavieros, George and Villeneuve, Aurélie and Vahlas, Constantin *Nanocomposite thin film of Ag nanoparticles embedded in amorphous Al<sub>2</sub>O<sub>3</sub> on optical sensors windows: Synthesis, characterization and targeted application towards transparency and anti-biofouling.* (2017) Surface and Coatings Technology, vol. 328. pp. 371-377. ISSN 0257-8972

Any correspondence concerning this service should be sent to the repository administrator:  
[staff-oatao@inp-toulouse.fr](mailto:staff-oatao@inp-toulouse.fr)

# Nanocomposite thin film of Ag nanoparticles embedded in amorphous Al<sub>2</sub>O<sub>3</sub> on optical sensors windows: Synthesis, characterization and targeted application towards transparency and anti-biofouling

C. Tendero<sup>a</sup>, A.-M. Lazar<sup>a</sup>, D. Samélor<sup>a</sup>, O. Debieu<sup>a</sup>, V. Constantoudis<sup>b,c</sup>, G. Papavieros<sup>b,c</sup>, A. Villeneuve<sup>d</sup>, C. Vahlas<sup>a,\*</sup>

<sup>a</sup> CIRIMAT, 4, allée Emile Monso, BP-44362, 31030 Toulouse Cedex 4, France

<sup>b</sup> Institute of Nanoscience and Nanotechnology, NCSR Demokritos, Neapoleos 10, 15310 Ag. Paraskevi, Greece

<sup>c</sup> Nanometrisis, TEPA Lefkippos, Patriarchou Grigoriou & Neapoleos 27, PO Box 60037, 15341 Agia Paraskevi, Greece

<sup>d</sup> ANDRA, 55290 Bure, France

## ABSTRACT

Increased motivation for environmental monitoring requires robust and reliable sensors. The present work aims at increasing the service time of optical sensors immersed in riverine waters by decreasing the development of biofouling on their surface. In this aim, nanocomposite coatings composed of metallic silver nanoparticles embedded in an amorphous alumina are co-deposited on sensor glass windows by chemical vapor deposition. Immersion for one week in the Saulx river, France, revealed a threefold decrease of biofouling on their surface compared with untreated glass surfaces while maintaining transparency. Such coatings can be considered as part of integrated tools, including for example mechanical cleaning, to reduce the maintenance of optical sensors immersed in riverine waters.

### Keywords:

Antibiofouling coatings

Transparent coatings

Optical sensors

Chemical vapor deposition

Amorphous alumina

Silver nanoparticles

## 1. Introduction

The protection of environmental sensors is an important issue in so far as such sensors have to operate continuously and autonomously during several months to collect high quality data [1]. In the case of immersed marine and riverine sensors, aquatic biofouling; i.e. microbial adhesion and biofilm formation, decreases the operating lifetime and increases the cost of maintenance of the sensor, since the sensor must be removed from the sampling location to be cleaned.

Particularly, in the case of optical sensors which are often implemented to monitor turbidity and nutrients such as chlorophyll, biofouling is one of the most prevalent hindrances to long-term, continuous, and in situ optical measurements because build-up of residue on the optical window causes degradation of measurement signals over time, hence reducing measurement accuracy [2]. The degradation of the optical performance in short time period spanning from days to months has been a concern since more than twenty years [3,4], resulting in the development of antifouling measures to prevent the deterioration of the optical window transparency of the sensor. Such measures may involve incorporation of some type of brush or wiper, however it should be

ensured that it will not scratch the optical surface. In this perspective, copper plates, tubing and shutters were proposed by Manov et al. to delay biofouling [5]. Chlorination resulting from either bleach injection or electrolysis [6] or the use of pressurized fresh water cleaning [7] have also been reported as means of chemical cleaning of sensors' lens and housing.

Anti-biofouling coatings may also be applied on the surface of optical lenses and windows as an alternative or complementary solution to the above ones [3]. In that case, the measurement medium and the sensor sensitive area must remain as much as possible unmodified. This implies that the coatings need to be transparent and to present low surface roughness to avoid erroneous measurements [2,5]. For sensors operating in marine environment, these specifications have been met through the use of conductive, catalytic coatings composed of platinum, Pt and indium tin oxide, ITO [8]. In this report, the electrocatalysis capability of Pt/ITO is used for the generation of Cl<sub>2</sub> from NaCl in seawater, without, however information provided on the transparency of the film. Alternatively, exposure of the optical instrument to ultraviolet radiation, UVR during short, though frequent maintenance periods can be used as a potential tool to control biofouling [9]. The authors report that intensity of UVR, but mostly duration of exposure in an hourly cycle (thus impacting operation time) are the most critical parameters to slow down the development of biofouling. Delauney and Compère [1]

\* Corresponding author.

E-mail address: [constantin.vahlas@ensiacet.fr](mailto:constantin.vahlas@ensiacet.fr) (C. Vahlas).

and more recently, Zhang and Zhang [10] compiled the various lens-cleaning techniques which have been studied by academia and optical sensor manufacturers.

Anti-biofouling coatings on glass windows immersed in riverine or continental water remain poorly developed up to now. Such coating architectures designed on purpose may include biocide nanoparticles, (NPs hereafter), like silver, Ag, supported on, or embedded in an optically transparent, smooth coating. This support may not only serve as a fixing medium of the Ag NPs. Indeed, Chang et al. reported that, in the case of an *Escherichia coli* bactericidal mechanism, unsupported  $\text{Ag}^+$  ions did not play an important role in the bactericidal process [11]. In contrast, when supported on gamma alumina,  $\gamma\text{-Al}_2\text{O}_3$ , a synergistic effect occurs between Ag and  $\gamma\text{-Al}_2\text{O}_3$ , illuminating a bactericidal mechanism promoted by catalytic oxidation. It is well known that the catalytic activity of  $\gamma\text{-Al}_2\text{O}_3$  is due to penta-coordinated  $\text{Al}^{3+}$  ions which are located on the surface of  $\gamma\text{-Al}_2\text{O}_3$  [12].

The authors group has developed various chemical vapor deposition, CVD processes for the production of amorphous alumina,  $\alpha\text{-Al}_2\text{O}_3$  films [13–15]. Such films, processed from aluminum tri-isopropoxide, ATI contain a large percentage of penta-coordinated  $\text{Al}^{3+}$  ions, as was demonstrated by  $^{27}\text{Al}$  nuclear magnetic resonance, NMR spectroscopy [16]. The group also investigated CVD processes of nanostructured composite coatings containing Ag NPs embedded in a titanium dioxide matrix [17].

Based on this information, an original, one step CVD process is presented hereafter which consists in the co-deposition of Ag NPs and of  $\alpha\text{-Al}_2\text{O}_3$ . It is aimed the formation of a nanocomposite coating where the Ag NPs are likely to ensure a biocide effect and the  $\alpha\text{-Al}_2\text{O}_3$  matrix stabilizes the NPs and serves as a catalytic support with limited, still acceptable impact on transparency. The adopted architecture of the nanocomposite coating consists in a first sublayer of pure  $\alpha\text{-Al}_2\text{O}_3$  on the glass window, followed by the major part of the coating, composed of Ag NPs embedded in  $\alpha\text{-Al}_2\text{O}_3$ . In this architecture, the sublayer ensures intimate contact with the glass surface and hence sufficient adhesion during the immersion tests; this is not the case for the composite film codeposited directly on the glass substrate. The main part of the coating serves as a reservoir of Ag NPs, which are exposed to the water through the evolving free surface during the lifetime of the low wear resistant coating. Indeed, the hardness  $H$  and the elastic modulus  $E$  of  $\alpha\text{-Al}_2\text{O}_3$  are  $10.8 \pm 0.8$  GPa and  $155 \pm 6$  GPa, respectively [18]. The resulting value of the elastic strain to failure  $H^3/E^2$  which is an indicator of wear resistance [19] equals 0.05 GPa. While applications involving mechanical contact require materials with a tenfold higher  $H^3/E^2$  values, the present one reveals a material which can be considered as sacrificial in low mechanical load operating environment, such as sediments-rich water flow. Such evaluation of  $\alpha\text{-Al}_2\text{O}_3$  coatings is supported by recent results, reporting that, when subjected to severe hydrothermal ageing, they are eroded resulting in the increase of their superficial roughness and porosity without, however affecting their adhesion on glass [15]. For these reasons, it is expected that applying a pure  $\alpha\text{-Al}_2\text{O}_3$  sublayer by the surface and loading a large external part of the host,  $\alpha\text{-Al}_2\text{O}_3$  coating with Ag NPs, should be beneficial to the maintaining of the expected anti-biofouling function of the surface and to the durability of the coating on the glass window.

Coated and as received optical windows were tested by immersion in an area belonging to a large monitoring network of the surface water quality within the frame of long term environmental observatory (OPE) of the French national radioactive waste management agency (ANDRA). One of the rivers whose quality is monitored within the OPE is the Saulx river (GPS  $48^\circ 24' 50''$  N,  $5^\circ 21' 35''$  E). The in situ tests were conducted on a site located upstream the Saulx, at the Echenay village. This observatory has been designed by ANDRA to provide a comprehensive and integrated description of the environment surface dynamics within the large Cigéo project (deep geological storage area of high level and long lifetime radioactive waste). The OPE is aimed at identifying environmental evolutions at relevant scales of space (local, regional or global) and to discriminate their origins

(natural, human activities...), in particular those from Cigéo. Relevant chemical and physical parameters as well as bio-indicators were identified to properly describe the environment. These indicators require continuous monitoring stations that are equipped with sensors. This work focuses on the protection of one of those commercial optical sensors (Bionef-BBE-Algae-torch) that measures relevant parameters such as the fluorescence intensity at  $680 \pm 100$  nm of chlorophyll and cyanobacteria after excitation at 470, 525, and 610 nm.

The paper is organized as follows: the CVD protocol for the deposition of the nanocomposite coating and the characterization techniques, including the evaluation of biofouling, are first detailed. Then, the microstructural characteristics of such coatings are determined. Finally, the optical transmission properties of the coated glass and the development of biofouling on the samples after immersion in riverine water are presented prior providing concluding remarks.

## 2. Materials and methods

### 2.1. Thin film deposition

Ag NPs were processed by direct liquid injection, DLI-CVD from silver pivalate  $(\text{CH}_3)_3\text{CC}(\text{O})\text{OAg}$  (namely AgPiv), by adapting a protocol reported in [17]. The precursor solution was prepared by mixing AgPiv (Lotus Synthesis) and a solution of mesitylene/dipropylamine (Sigma Aldrich) (90/10 vol. respectively) inside a Schlenk flask, resulting in a  $10^{-2}$  M AgPiv solution. Then, the Schlenk flask was connected with the injection system and purged several times with pressurized  $\text{N}_2$  (99.9999%, Praxair, for all  $\text{N}_2$  lines of the experimental setup). DLI of the solution was carried out with a Kemstream Vapbox® system composed of two injectors connected in series. One gas line was connected to the Schlenk flask. The frequency and opening times (typically 1 Hz and 10 ms) of the injection system were controlled by a computer interface to feed the thermally regulated evaporation chamber with precursor solution microdroplets mixed with  $\text{N}_2$  gas, having a flow set of 320 standard cubic centimeters per minute (scm).

$\alpha\text{-Al}_2\text{O}_3$ , was deposited from ATI following a protocol reported in [20]. ATI (>98%, Acros Organics) was melted in a bubbler above 413 K and then was maintained supercooled at 373 K. It was transported to the deposition zone by bubbling 30 scm of  $\text{N}_2$  (regulated, as for all other gas lines by mass flow controllers) through the bubbler.

The injected AgPiv solution, the vaporized ATI and an additional  $\text{N}_2$  dilution line flowing at 100 scm were simultaneously introduced in a homemade horizontal hot-wall CVD reactor. All lines were heated at 373 K to prevent the condensation of precursors. The reactor is composed of a fused-silica tube (25 mm diameter, 300 mm length) heated by a resistive furnace. A dry pump and pressure gauges connected to the output of the fused-silica tube were used to control the deposition pressure to 5 Torr.

Four, 1 cm thick glass samples of the Bionef-BBE-Algae-torch commercial sensor external windows were placed on a row from Q1 in the beginning to Q4 at the end of the isothermal zone of the furnace. Silicon substrates ( $10 \times 10$  mm) cut from 4" Si (001) wafers (Sil'tronix-ST), placed at intermediate positions, were also coated and used for TEM analysis. We have already demonstrated that the characteristics of  $\alpha\text{-Al}_2\text{O}_3$  films are independent of the nature of the substrate, namely AISI 304 L stainless steel (SS), (100) oriented Si wafers, and thermally grown silica on Si wafers [13]. All samples were cleaned in an ultrasonic bath with acetone and ethanol, and were immediately introduced to the reactor. Co-deposition was performed at 723 K for 31 min to reach submicrometric thickness (ranging from 300 nm to 200 nm for Q1 to Q4 respectively, estimated by reflectometry measurements). This temperature is suitable for the deposition of both Ag NPs [17] and  $\alpha\text{-Al}_2\text{O}_3$  films [20] from the two selected precursors. Prior codeposition, a thin film of pure  $\alpha\text{-Al}_2\text{O}_3$  was deposited on the substrates surface with the aim to enhance the adhesion, by feeding the reactor with ATI and the dilution gas for 5 min, in the previously defined conditions. The deposition

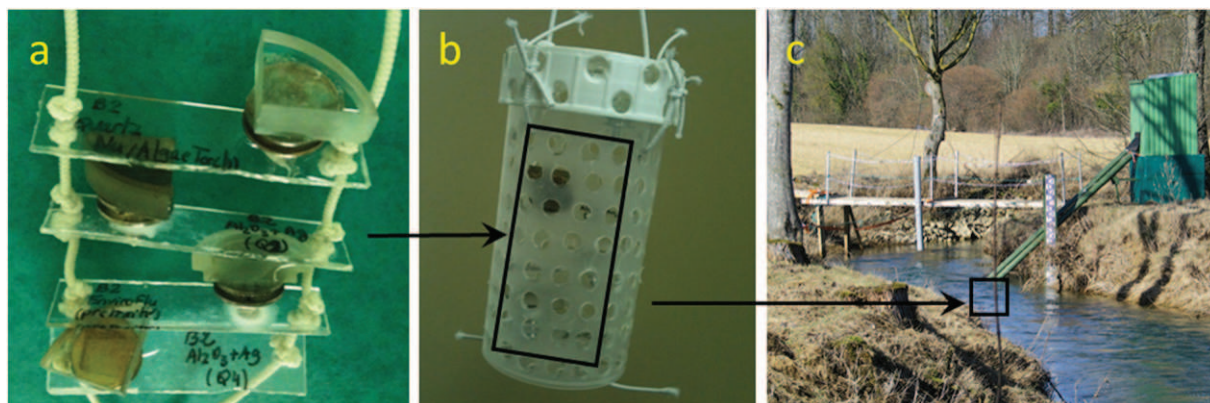


**Fig. 1.** Positioning of the samples inside the container prior immersion (a). Immersed plastic container with the samples (b). Location of the samples immersion area upstream the Saulx, near the Echenay village France (c).

process was terminated by first switching off either the ATI or the AgPiv flow so as to respectively obtain an Ag-rich surface to enhance anti-biofouling activity or an alumina-rich surface for the samples used for transmission electron microscopy, TEM (to ensure the integrity of the coating during cross section preparation).

## 2.2. Materials characterization and tests

Surface morphology was observed by scanning electron microscopy (SEM) on a LEO 435VP instrument. SEM samples were covered by a thin layer of sputtered gold to prevent charging effects. Atomic force microscopy (AFM) was used in a tapping™ mode on an Agilent 5500 device to evaluate the roughness. Cross sections of the films deposited on Si were prepared by cutting the samples into two thin slices (normal to the interface coating/substrate) with a diamond wire saw. The slices were glued together, coating to coating, and embedded in a 3 mm diameter brass tube in an epoxy resin. After curing, the tube was sectioned into approximately 300  $\mu\text{m}$  thick discs which were polished on both faces and dimpled before ion-milling to transparency with a Precision Ion Polishing System. Cross section samples were imaged by Transmission Electron Microscopy (TEM) with a JEOL JEM-2010F microscope operating at 200 kV and equipped with a BRUKER Energy Dispersive Spectrometer (EDS) for the investigation of the nature, the size and

crystalline structure of Ag-NPs. X-ray Photoelectron spectroscopy (XPS) measurements were performed on a Thermo Scientific K-Alpha instrument capable of a typical base pressure of  $10^{-9}$  Torr, using monochromatic Al  $K_{\alpha}$  radiation (1486.7 eV). The spectrometer energy calibration was performed using the Au  $4f_{7/2}$  ( $83.9 \pm 0.1$  eV) and Cu  $2p_{3/2}$  ( $932.7 \pm 0.1$  eV) photoelectron lines. Charging compensation and neutralization were applied by using a dual beam flood gun. The diameter of the probed areas was ca. 400  $\mu\text{m}$ . Constant pass energy of 30 eV and energy steps of 0.1 eV were used for high-resolution scans. Surface erosion was realized using Ar ions accelerated at 2 keV, resulting for  $\alpha\text{-Al}_2\text{O}_3$  in an erosion rate of about 0.08 nm/s [21]. The atomic concentrations were determined from photoelectron peak areas using the atomic sensitivity factors reported by Scofield, taking into account the transmission function of the analyzer. UV-Vis-NIR transmittance spectra were measured by a Perkin-Elmer Lambda-19 spectrophotometer with an incidence angle of  $8^\circ$ .

Bare and surface treated optical glass windows were glued on metallic dots, which in turn were glued on a glass support: this set-up was aimed at preventing biofouling contamination of the samples coming from non-treated supports as already observed in previous immersion campaigns. This set-up was then conditioned in a plastic container and immersed in the Saulx river during one week, which is long enough to test the protective coating antifouling efficiency during the early stages of biofouling growth. Fig. 1 presents a series of photographs

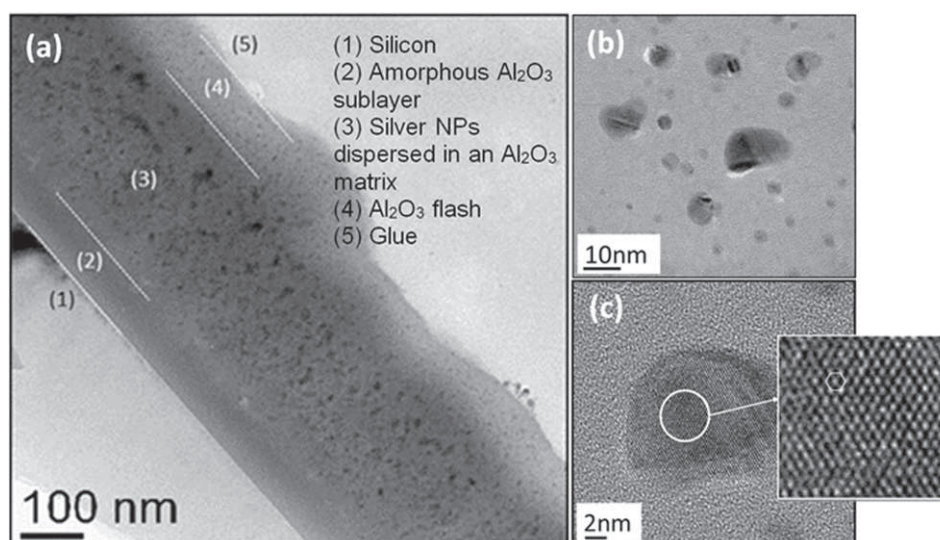


**Fig. 2.** (a) Bright field TEM micrograph of a cross section of a representative  $\alpha\text{-Al}_2\text{O}_3/\text{Ag}$  NPs composite coating with an  $\alpha\text{-Al}_2\text{O}_3$  rich top-layer, deposited on Si. (b) and (c) High-Resolution TEM micrographs illustrating Ag NPs dispersed in  $\alpha\text{-Al}_2\text{O}_3$ . The insert in (c) highlights the [111] orientation of an fcc-crystallized Ag NP. The spacing between the (110) reticular planes is 0.290 nm.

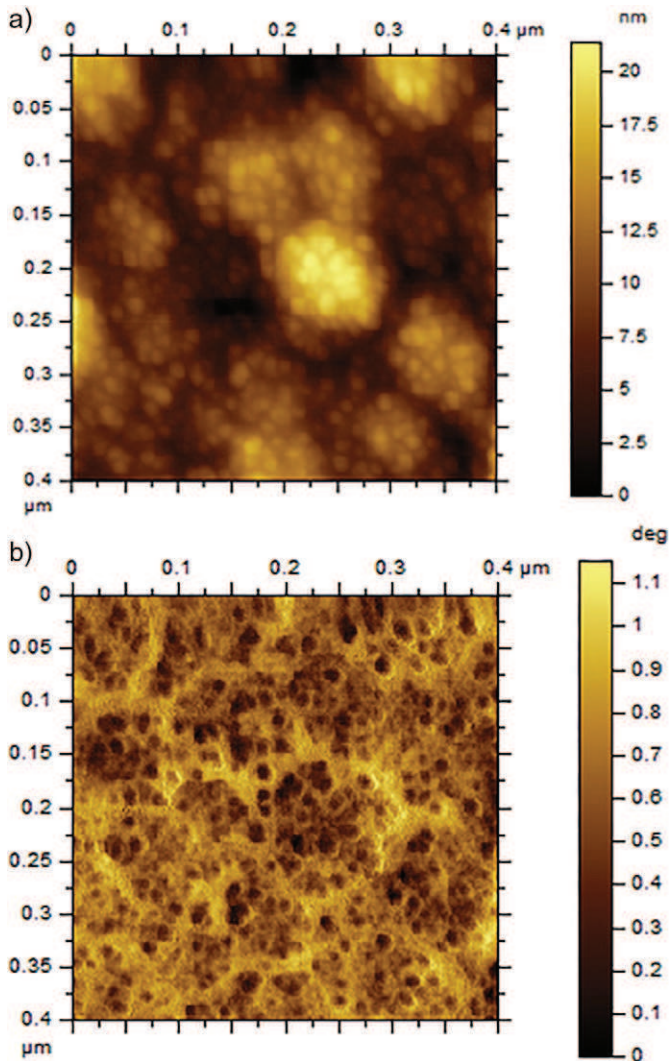


**Fig. 3.** Atomic Force Microscopy pictures of the surface of coating similar to Q4, i.e.: AgNPs embedded in a- $\text{Al}_2\text{O}_3$  matrix with an Ag rich top-layer. (a) Topography signal leading to an arithmetic roughness,  $S_q$ , of 5 nm. (b) Phase-shift mapping that highlights the contrast between AgNPs and a- $\text{Al}_2\text{O}_3$  matrix.

which illustrate the conditioning of the samples and the location of their immersion.

The anti-biofouling efficiency was evaluated by analysing top-down SEM images of bare and coated samples using nanoTOPO\_SEM™ software provided by Nanometrisis. The key idea of the analysis is based on the fact that biofouling adds roughness on sample surfaces and therefore the resulting slope and height of the features is manifested by the bright areas in SEM images comprising pixels with large intensity values. This means that we can quantify estimate the biofouling amount by measuring the fraction of bright areas in the SEM images of samples. To this end, first appropriate image processing (detrrending, cropping ...) is applied to homogenize images and their intensity fields. Then, the fraction of bright areas in the homogenized SEM images is estimated by measuring the number of pixels with intensities larger than a properly chosen threshold and by normalizing them to the total number of pixels in the analysed image. In this process, various reasonable bright/dark thresholds are used and the obtained results are compared and compiled to get the final conclusions.

### 3. Results and discussion

Q1 to Q4 coated samples are characterized regarding their morphology, structure, optical transmittance and antifouling properties. TEM is

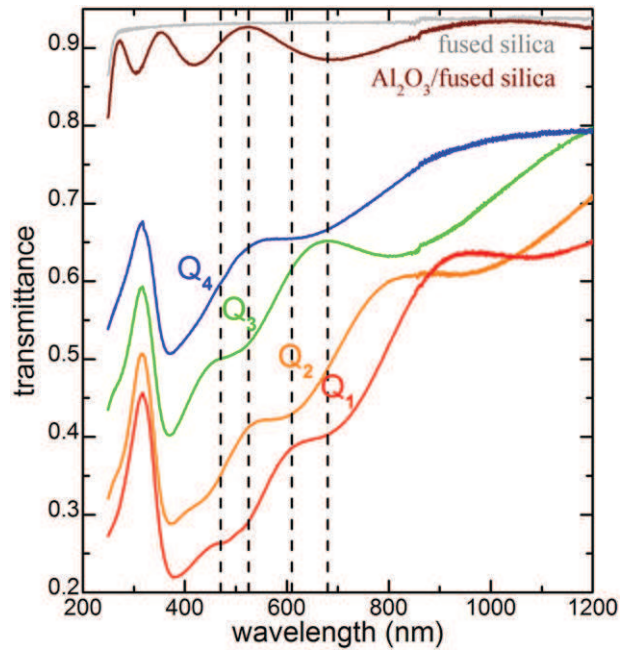


**Fig. 4.** Transmittance spectra of the Q1 to Q4 coatings. Fused silica window and a- $\text{Al}_2\text{O}_3$  deposited on fused silica are shown for comparison. The four dotted lines point on the wavelengths used by the sensor.

performed on a a- $\text{Al}_2\text{O}_3$ /Ag NPs composite coating to evaluate its nanostructure and to obtain data on the morphology, size and crystalline structure of the Ag NPs. The coating is deposited on silicon instead of glass to facilitate the sample preparation, with an alumina rich top-layer. On the bright field TEM cross section micrograph (Fig. 2a) a 70 nm thick a- $\text{Al}_2\text{O}_3$  sub-layer (2) is observed on the Si substrate (1), followed by a 260 nm thick layer consisting of Ag NPs (black dots) embedded in a- $\text{Al}_2\text{O}_3$  (3). The external part of the coating is composed of a ca. 75 nm thick a- $\text{Al}_2\text{O}_3$  sub-layer (4). In Fig. 2b one can observe the Ag NPs. Their size distribution is monodisperse centered at 6 nm. Fig. 2c shows a high resolution TEM micrograph of one Ag NP and the insert in this figure reveals the fcc compact stacking of Ag, perfectly oriented in the [111] direction, with a lattice spacing of 0.290 nm between the (110) planes in agreement with the reference value of 0.289 nm [22].

Fig. 3a presents an AFM topography image of a sample similar to Q4 (with an Ag NPs rich a- $\text{Al}_2\text{O}_3$  toplayer). The scanned surface area of  $400 \times 400 \text{ nm}^2$  reveals a two scale microstructure: a nodular one, with ca. 90 nm nodules size, on the top of which are smaller features, attributed to Ag NPs, whose size does not exceed 10 nm. The micrograph of Fig. 3b is the phase-contrast image of the same area. The contrast between the two scale features is enhanced due to their different interaction of the Ag NPs and  $\text{Al}_2\text{O}_3$  with the AFM probe resulting in a different phase shift with the free-oscillation signal. The quadratic roughness ( $S_q$ ) of the surface is  $5.0 \pm 0.5 \text{ nm}$ , averaged over 10 images, to be compared with the slightly lower  $S_q$  of the bare substrate,  $0.8 \pm 0.2 \text{ nm}$ . Such moderate increase of the roughness shouldn't affect the sensor operation and will be taken into account during its calibration phase.

Fig. 4 shows the optical transmittance spectra of the four nanocomposite films Q1 to Q4 before immersion. The four dotted lines point on the wavelengths used by the sensor. All four spectra consist of a transmittance band peaking at a fixed position of 315 nm and a broad absorption band covering the vis-NIR spectral domain which contains several interference fringes. The fixed transmittance band results from the minimum of the imaginary part of the refractive index of bulk Ag  $k_{\text{Ag}}$  [23] due to Ag interband transitions from 3.83 eV (323 nm) to higher

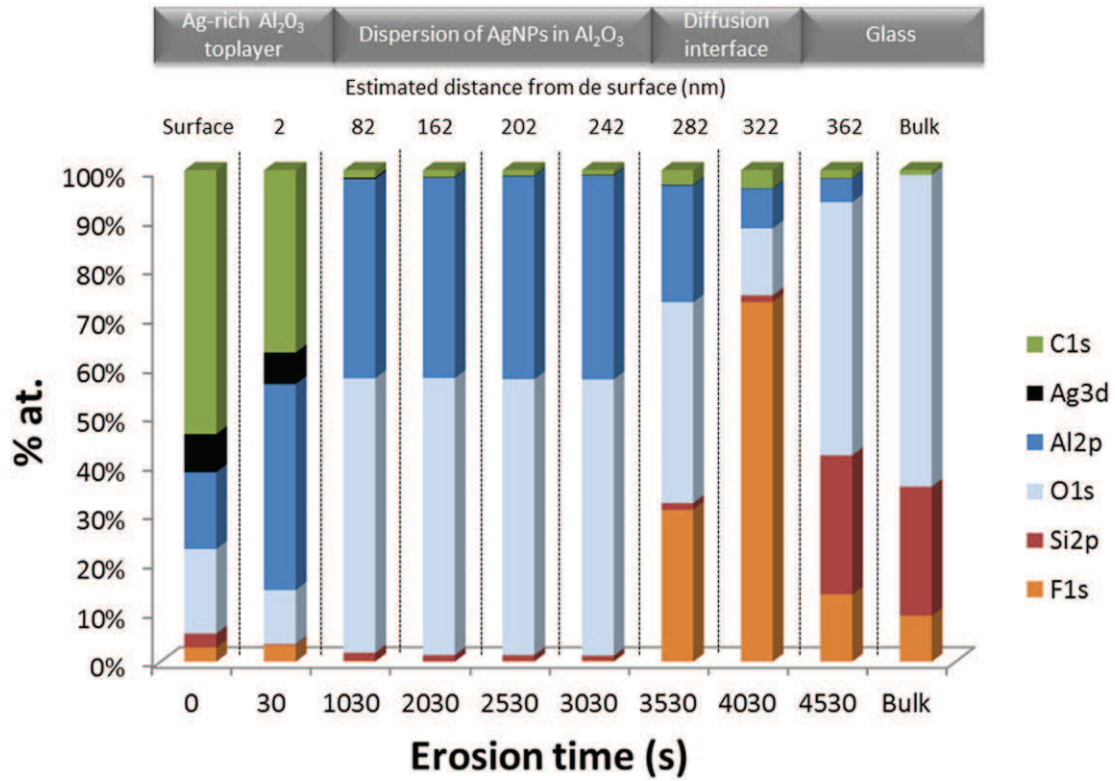


Fig. 5. XPS analysis of Q4 chemical composition (at.%) as a function of erosion time.

energies [24]. The transmittance band intensity gradually increases from Q1 to Q4, due to the decrease of the film thickness, attributed to the precursor consumption and hence to a declining concentration gradient from the entrance to the exit of the deposition zone in the reactor. Thickness increase results in the increase of the absorption since the imaginary part of the resulting effective refractive index of the medium composed of Ag NPs ( $k_{Ag} \neq 0$ ) and  $Al_2O_3$  ( $k_{alumina} = 0$ ) host media is non null. Besides, the gradual displacement of the interference fringes

towards longer wavelengths is also characteristic of the film thickness increase. The absorption band originates from surface plasmon resonance of Ag NPs which is known to occur between 350 and 800 nm in  $Al_2O_3$  environments [25,26]. The transmittance at the four wavelengths of interest for sample Q4 is between 0.5 and 0.7. This degradation of the transmittance can be reduced through appropriate tuning of the characteristics of the coating, namely its thickness, and the density and size of the Ag NPs, while maintaining the anti-biofouling efficiency (see next section). Since the four samples were processed in the same batch, it is expected that the size, density, and shape of Ag NPs do not

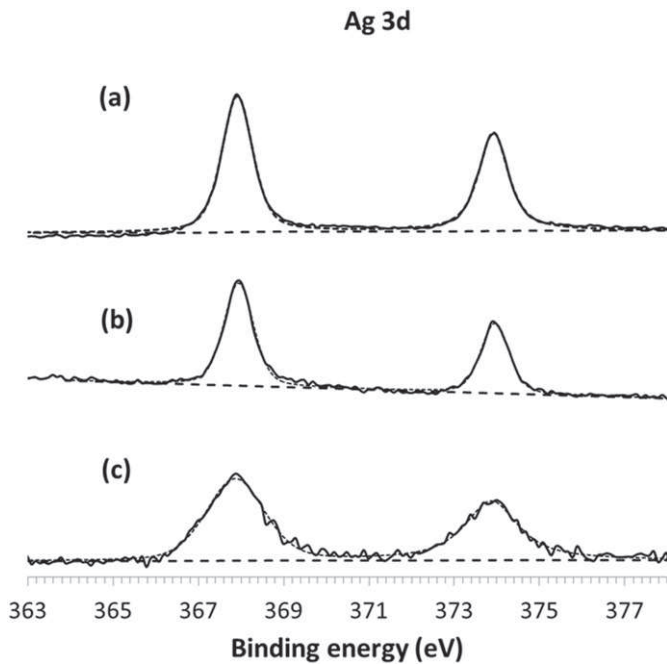


Fig. 6. Ag 3d X-ray photoelectron spectra as deposited (a), after erosion for 30 s (b) and 1030 s (c) of sample Q4.

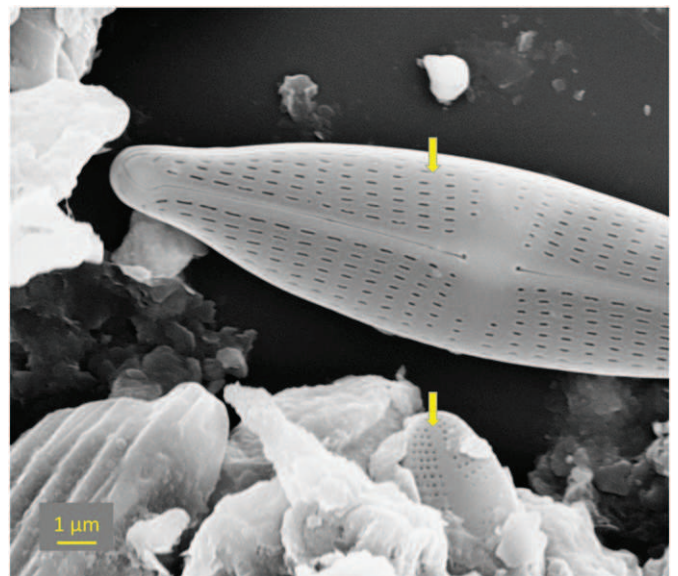
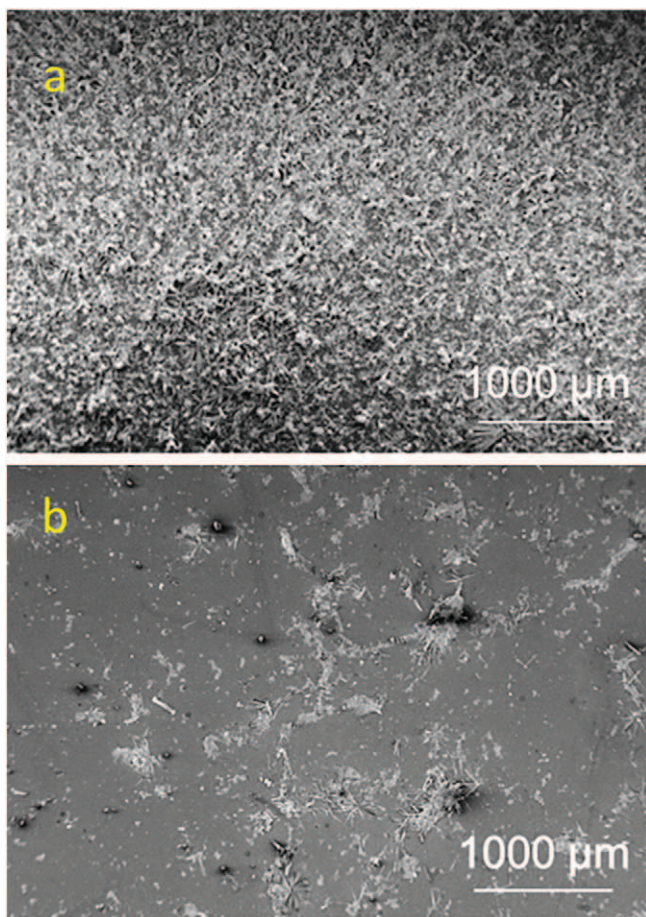


Fig. 7. SEM surface micrograph of a bare glass window after immersion, illustrating the development of fouling. Both minerals (left and lower part of the image) and microorganisms, namely diatoms (arrowed) are present.



**Fig. 8.** SEM surface micrographs of bare (a) and coated (b) glass samples after one week immersion.

significantly change in the four films. This is confirmed by the fact that the surface plasmon absorption maxima are all localized at ca. 370 nm and by the fact that the broad band seems to roughly have the same width (if one disregards the interference fringes).

Fig. 5 presents the XPS depth profile of sample Q4 after immersion. The profile confirms the coating structuration targeted by the deposition conditions by revealing (a) a first, ca. 3 nm external zone, (b) a main part, whose thickness is in the order of 300 nm, (c) a ca. 50 nm thick interdiffusion zone and finally (d) the glass substrate. The overall thickness for sample Q4 is estimated 350 nm by considering an erosion rate of 0.08 nm/s for  $\alpha\text{-Al}_2\text{O}_3$ , to be compared with the value of 200 nm estimated by reflectometry. This difference is attributed to uncertainties of the two methods, namely the erosion rate for XPS and the optical index for reflectometry. The thin external zone is composed of C, O, Ag and Si. Ag corresponds to the coating top-layer whereas carbon, silicon and oxygen are attributed both to the contamination of the extreme surface and to the micro-organisms which adhered on the surface during the immersion test. The main part of the coating consists of aluminum oxide which is homogeneous through the coating depth as the ratio of Al and O signals remains constant. The Ag signal is detected and it is close to the XPS quantification limit (0.1% at.).

The high resolution XPS signal of Ag3d is further studied to identify the oxidation state of the Ag NPs in the matrix. The Ag3d XPS spectra shown in Fig. 6 illustrate the bonding energies of  $\text{Ag}3d^{3/2}$  and  $\text{Ag}3d^{5/2}$  on the surface (Fig. 6a) and inside the coating after 30 s (Fig. 6b) and 1030 s (Fig. 6c) of erosion. The binding energies of  $\text{Ag}3d^{3/2}$  and  $\text{Ag}3d^{5/2}$  are 374.05 eV and 368.04 eV respectively, with a splitting of the 3d doublet that is close to 6 eV, in agreement with the literature [27]. These results confirm the TEM results, according to which the Ag in

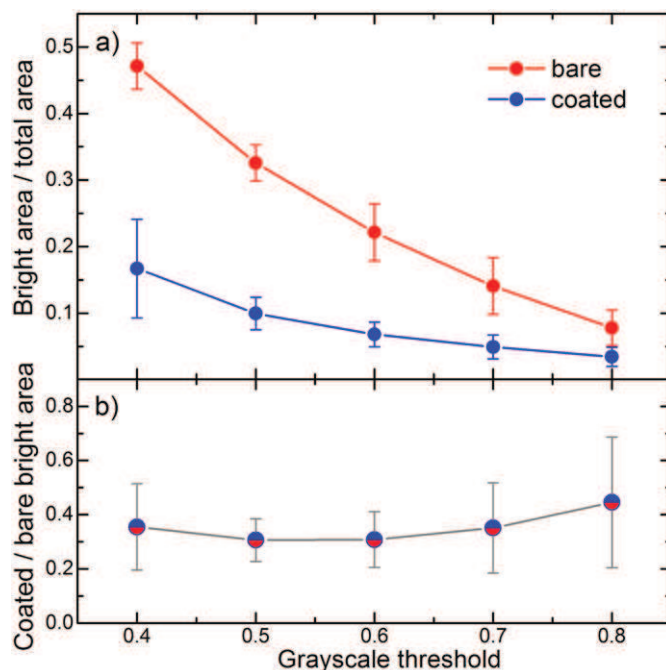


**Fig. 9.** a) Bright area over total area ratios of bare and coated glass samples for a wide range of grayscale thresholds used in the analysis of SEM images, b) coated over bare bright area ratio as a function of the grayscale threshold. The error bars indicate the uncertainty of measurements in different images.

the nanocomposite coating is in the metallic state  $\text{Ag}^0$ . However, due to the low signal-over-noise ratio, the presence of  $\text{Ag}^+(\text{I})$  at the interface Ag NPs/alumina cannot be excluded. Finally, the interface between the coating and the glass substrate reveals the diffusion of fluorine and magnesium within the coating. Similar results are obtained for the other samples, Q1, Q2 and Q3.

Visual observation of the samples surface after immersion reveals significant differences between untreated and coated samples. The former present uniform, intense development of biofouling, which covers the entire surface of the samples. The surface of the latter is partly covered, with large parts remaining unaffected. In both cases, the fouling consists of minerals and micro-organisms such as diatoms, as shown in Fig. 7.

A closer observation of the samples surface was performed by SEM through surface micrographs probing a 15 mm<sup>2</sup> surface area. Fig. 8 presents such two large scale micrographs, of bare (Fig. 8a) and coated (Fig. 8b) glass surfaces after immersion. The observed surfaces confirm the visual observations of the samples, namely the complete coverage by microorganisms of the surface of the untreated sample in contrast to the limited, and localized development of biofouling on the surface of the coated one.

Quantitative assessment of the biofouling fraction can be made by measuring the fraction of bright areas of SEM micrographs of four bare and four (Q1-Q4) coated samples following the procedure described in the Materials and methods section. The results of the micrographs' analysis are shown in Fig. 9a where the biofouling fraction is plotted for various grayscale thresholds (0.4–0.7) used to define the bright areas. In addition to an expected decrease of measured biofouling vs. grayscale threshold, one can notice that, for all grayscale thresholds, the biofouling fraction of coated samples is systematically and unambiguously lower than that of bare samples. To quantify this decrease, in Fig. 9b we plot the ratio of biofouling of coated to the biofouling of bare samples for four grayscale thresholds. The value of this ratio is included between  $0.30 \pm 0.10$  and  $0.35 \pm 0.17$ ; it does not monotonically vary with the value of the grayscale threshold. It is concluded that CVD nanocomposite thin films of Ag NPs embedded in  $\alpha\text{-Al}_2\text{O}_3$  are efficient in decreasing biofouling on glass windows.



The present proof of principle paves the way to further improvement of the anti-biofouling efficiency by optimizing coating characteristics, such as the coating thickness and the Ag NPs concentration, through the fine tuning of the process conditions. The appropriate guide for this optimization would be the monitoring of the optical transmittance with the immersion time. Such coatings can thus be considered as part of integrated tools, including for example mechanical cleaning, to reduce the maintenance of optical sensors immersed in riverine waters [28]. The cost of this thermally activated CVD process is limited since the deposition temperature of 723 K (450 °C) is moderate, a small quantity of AgPiv is involved and ATI, the main chemical, is inexpensive.

#### 4. Conclusions

Nanocomposite coatings consisting of silver nanoparticles embedded in amorphous alumina were deposited on commercial glass windows aiming at the protection against biofouling of optical sensors immersed in riverine waters. The coatings were processed by an integrated CVD process, through codeposition of Ag from AgPiv and of  $\text{Al}_2\text{O}_3$  from ATI at 623 K and 5 Torr. The transmittance in the visible range ranges from 0.5 to 0.7 or the thinnest, 200 nm thick films. After immersion for one week in the Saulx river, France, a threefold decrease of the percentage of the surface of these samples covered by microorganisms was observed, compared with the biofouling development on untreated surfaces. The critical function of biofouling delay being demonstrated, future perspectives of this proof of principle include correlation among (i) the coatings' characteristics, including thickness, roughness and Ag NPs size and concentration, (ii) the targeted functionalities, namely optical transmittance and anti-biofouling, and (iii) the durability of the functionality during the sacrificial erosion of the coating. This correlation can only be investigated through longer immersion campaigns of the coated windows which should be mounted on the sensor so as to monitor the quality of the optical measurement and its evolution with time for given hydraulic, biological and environmental specifications.

#### Acknowledgments

This work was financially supported by ANDRA (Bure, France) under the ANDRA/053441 project grant, and by the Fondation STAE (Sciences et Technologies pour l'Aéronautique et l'Espace) (RTRA-STAE/2008/PS/006) project "MAISOE" (Microlaboratoires d'Analyses In Situ pour des Observatoires Environnementaux). The authors are indebted to M.C. Lafont, CIRIMAT for the TEM characterization, to J. Esvan, CIRIMAT for XPS analysis and to Ph. Behra, INPT for his continuous support.

#### References

- [1] L. Delauney, C. Compère, M. Lehaitre, Biofouling protection for marine environmental sensors, *Ocean Sci.* 6 (2010) 503–511.
- [2] A. Whelan, F. Regan, Antifouling strategies for marine and riverine sensors, *J. Environ. Monit.* 8 (2006) 880–886.
- [3] R.M. Head, J. Davenport, J.C. Thomason, The effect of depth on the accrual of marine biofilms on glass substrata deployed in the Clyde Sea, Scotland, *Biofouling* 20 (2004) 177–180.
- [4] S. Bhatia, D. Risk, A. Pustam, T. Smith-Palmer, G. Burton, L. Melo, P. Wild, Biofouling of an all-optical sensor for seafloor monitoring of marine carbon capture and storage

- sites, in: T. Dixon, H. Herzog, S. Twinning (Eds.) 12th International Conference on Greenhouse Gas Control Technologies, Ghgt-12, 2014, pp. 3848–3852.
- [5] D.V. Manov, G.C. Chang, T.D. Dickey, Methods for reducing biofouling of moored optical sensors, *J. Atmos. Ocean. Technol.* 21 (2004) 958–968.
- [6] L. Delauney, C. Compère, An example: biofouling protection for marine Environmental sensors by local chlorination, in: H.-C. Flemming, P.S. Murthy, R. Venkatesan, K. Cooksey (Eds.), *Marine and Industrial Biofouling*, Springer-Verlag, Berlin Heidelberg 2009, pp. 119–134.
- [7] J.R. Etheridge, F. Birgand, M.R. Burchell, B.T. Smith, Addressing the fouling of in situ ultraviolet-visual spectrometers used to continuously monitor water quality in brackish tidal marsh waters, *J. Environ. Qual.* 42 (2013) 1896–1901.
- [8] Y.X. Xue, J. Zhao, R. Qiu, J.Y. Zheng, C.G. Lin, B.J. Ma, P. Wang, In situ glass antifouling using Pt nanoparticle coating for periodic electrolysis of seawater, *Appl. Surf. Sci.* 357 (2015) 60–68.
- [9] J.S. Patil, H. Kimoto, T. Kimoto, T. Saino, Ultraviolet radiation (UV-C): a potential tool for the control of biofouling on marine optical instruments, *Biofouling* 23 (2007) 215–230.
- [10] Y.L. Zhang, N.Q. Zhang, Air-blast anti-fouling cleaning for aquatic optical sensors, *Int. J. Agric. Biol. Eng.* 8 (2015) 128–135.
- [11] Q.Y. Chang, L.Z. Yan, M.X. Chen, H. He, J.H. Qu, Bactericidal mechanism of  $\text{Ag}/\text{Al}_2\text{O}_3$  against *Escherichia coli*, *Langmuir* 23 (2007) 11197–11199.
- [12] J.H. Kwak, J. Hu, A. Lukaski, D.H. Kim, J. Szanyi, C.H.F. Peden, Role of pentacoordinated  $\text{Al}^{3+}$  ions in the high temperature phase transformation of gamma- $\text{Al}_2\text{O}_3$ , *J. Phys. Chem. C* 112 (2008) 9486–9492.
- [13] A. Gleizes, C. Vahlas, M.M. Sovar, D. Samélor, M.C. Lafont, Chemical vapor deposited aluminium oxide coatings from aluminium tri-iso-propoxide: correlation between processing conditions and composition, *Chem. Vap. Depos.* 13 (2007) 23–29.
- [14] L. Baggetto, C. Charvillat, J. Esvan, Y. Thébault, D. Samélor, H. Vergnes, B. Caussat, A. Gleizes, C. Vahlas, A process-structure investigation of aluminum oxide and oxycarbide thin films prepared by direct liquid injection chemical vapor deposition of dimethylaluminum isopropoxide (DMAI), *Chem. Vap. Depos.* 21 (2015) 343–351.
- [15] P.-L. Etchepare, L. Baggetto, H. Vergnes, D. Samélor, D. Sadowski, B. Caussat, C. Vahlas, Direct liquid injection chemical vapor deposition of amorphous alumina from aluminum tri-isopropoxide: thin film process, structure and properties, *Adv. Mater. Interfaces* 3 (2016) 1600014.
- [16] V. Sarou-Kanian, A.N. Gleizes, P. Florian, D. Samélor, D. Massiot, C. Vahlas, Temperature-dependent 4-, 5- and 6-fold coordination of aluminum in MOCVD-grown amorphous alumina films: a very high field  $\text{al}$ -27-NMR study, *J. Phys. Chem. C* 117 (2013) 21965–21971.
- [17] J. Mungkalasiri, L. Bedel, F. Emieux, J. Dore, F.N.R. Renaud, C. Sarantopoulos, F. Maury, CVD elaboration of nanostructured  $\text{TiO}_2$ -ag thin films with efficient antibacterial properties, *Chem. Vap. Depos.* 16 (2010) 35–41.
- [18] Y. Balcaen, N. Radutoiu, J. Alexis, J.D. Béguin, L. Lacroix, D. Samélor, C. Vahlas, Mechanical and barrier properties of MOCVD processed alumina coatings on TA6V titanium alloy, *Surf. Coat. Technol.* 206 (2011) 1684–1690.
- [19] A. Leyland, A. Matthews, On the significance of the H/E ratio in wear control: a nanocomposite coating approach to optimised tribological behaviour, *Wear* 246 (2000) 1–11.
- [20] M.M. Sovar, D. Samélor, A.N. Gleizes, C. Vahlas, Aluminium tri-isopropoxide: shelf life, transport properties, and decomposition kinetics for the low temperature processing of aluminium oxide-based coatings, *Surf. Coat. Technol.* 201 (2007) 9159–9162.
- [21] L. Baggetto, C. Charvillat, Y. Thébault, J. Esvan, M.C. Lafont, E. Scheid, G.M. Veith, C. Vahlas, Amorphous alumina thin films deposited on titanium: interfacial chemistry and thermal oxidation barrier properties, *Phys. Status Solidi A* 213 (2016) 470–480.
- [22] P. Villars, L.D. Calvert, W.B. Pearson, *Pearson's Handbook of Crystallographic Data for Intermetallic Phases*, Materials Park, OH, 1991.
- [23] X.K. Meng, T. S.C., S. Vongehr, A review on diverse silver nanostructures, *J. Mater. Sci. Technol.* 26 (2010) 487–522.
- [24] M. Fox, Introduction to nanophotonics, Sergey V. Gaponenko, *Contemp. Phys.* 52 (2011) 257.
- [25] S. Camelio, E. Vandenhecke, S. Rousselet, D. Babonneau, Optimization of growth and ordering of Ag nanoparticle arrays on ripple patterned alumina surfaces for strong plasmonic coupling, *Nanotechnology* 25 (2014), 035706.
- [26] A. Esteban-Cubillo, C. Diaz, A. Fernandez, L.A. Diaz, C. Pecharroman, Silver nanoparticles supported on  $\alpha$ -,  $\eta$ -, and  $\delta$ -alumina, *J. Eur. Ceram. Soc.* 26 (2006) 1–7.
- [27] B. Ajitha, Y. Ashok Kumar Reddy, P. Sreedhara Reddy, Biosynthesis of silver nanoparticles using *Momordica charantia* leaf broth: evaluation of their innate antimicrobial and catalytic activities, *J. Photochem. Photobiol. B* 146 (2015) 1–9.
- [28] J. Joslin, B. Polagye, Demonstration of biofouling mitigation methods for long-term deployments of optical cameras, *Mar. Technol. Soc. J.* 49 (2015) 88–96.